The 2010 IEEE/RSJ International Conference on
Intelligent Robots and Systems
October 18-22, 2010, Taipei, Taiwan

Combining Suppression of the Disturbance and Reactive Stepping for Recovering Balance

Mitsuharu Morisawa, Fumio Kanehiro, Kenji Kaneko, Nicolas Mansard, Joan Sola, Eiichi Yoshida, Kazuhiro Yokoi and Jean-Paul Laumond

Abstract— **This paper proposes a new framework to recover balance against external forces by combining disturbance suppression and reactive stepping. In the view point of the feedback control, a reactive step can help to diminish the disturbance caused by an external force that should be compensated to maintain balance. In other words, if the adequate step is performed, the feedback controller does not have to compensate all of the external force by itself. Under this concept, we propose an original solution to distribute the compensation between a feedback controller and a reactive step, according to the period of support phase and a disturbance characteristic. We first clearly distinguish between the role of the disturbance suppression and the reactive stepping. Then, based on this distinction, the small disturbance of external force or happening late during the single-support phase, is mainly suppressed by state feedback. The large disturbance which is out of capability by feedback controller and at the beginning of the single-support phase, is absorbed by modifying reactively the next steps. The proposed method is validated through experimental results with the HRP-2 humanoid robot.**

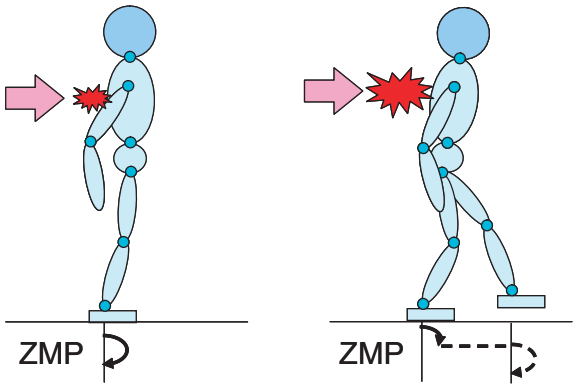

(a) Disturbance suppression (b) Reactive step

Fig. 1. Two motion strategies against external force

I. Introduction

There are two contrastive strategies to maintain balance for a humanoid robot: one is to suppress the disturbance by absorbing the external force using feedback control (Fig. 1 (a)). The other is a reactive step following the external force (Fig. 1 (b)). Although a small disturbance can be compensated with the appropriate feedback (such as compliant motion,) a large one will require a reactive step. However, a step motion is strongly constrained by temporal and physical restrictions. Therefore it is difficult to design a stabilization by a unified methodology.

Classically, there is a clear separation between the generation of the center of gravity (COG) and zero-momentum point (ZMP) on one side, and the feedback control on this trajectory of the other side [1]. This separation simplifies the planing phase at first approximation, since the robot with feedback can be considered to have a simple dynamics. However, this artificial decoupling turns the problem of deciding the next step to be very difficult when trying to really compensate for strong perturbations that require both feedback and stepping.

Mitsuharu. Morisawa, Fumio Kanehiro, Kenji Kaneko, Eiichi Yoshida, and Kazuhito Yokoi are with Research Institute of Intelligent Systems, National Institute of Advanced Industrial Science and Technology (AIST), 1-1-1, Umezono, Tsukuba, Ibaraki, 305-8568, Japan. {m.morisawa, f-kanehiro, k.kaneko, s.kajita, e.yoshida, Kazuhito.Yokoi}@aist.go.jp

Nicolas Mansard, Joan Sola and Jean-Paul Laumond are with LAAS-CNRS, University of Toulouse, 7 avenue du Colonel Roche, 31077 Toulouse, France. {nmansard, jsola, jpl}@laas.fr

Several works have been propose to trigger an adequate trajectory modification from the result of the feedback control. It was proposed in [2] to discretize a linear-inverted-pendulum model by step cycles under instantaneous changing of the support leg. Using this simplification, an appropriate landing position is computed by feedback on the COG position and velocity. Instead of only considering the COG, the angular momentum induced on the inverted pendulum can be used to compute the next foot position that counteract a strong disturbance [3]. In [4], it was proposed to update the COG trajectory in a short cycle using the preview control, using the output the feedback controller that tracks the ZMP reference.

On the other hand, several work have studied how to decide the best next-foot placement. The *Capture Point* computes a stable region for the inverted-pendulum-with-flywheel model under instantaneous torque [5]. Diedam proposes adaptive foot positioning under several constraints using a linear-model predictive control [6]. Finally, a humanoid robot that can recover from human-pushing disturbances during running in place has been presented in [7]. Takenaka proposes several balance control techniques which is to keep a ground reaction force [8]. In this method, as a result of the *model ZMP control* which accelerates the upper body, a landing position is modified locally.

In [9], we proposed to rely on an analytical solution of the linear invert pendulum, using piecewise polynomials of the ZMP. This solver is able to plan the COG and the ZMP trajectories in very short time, allowing to embed it in the

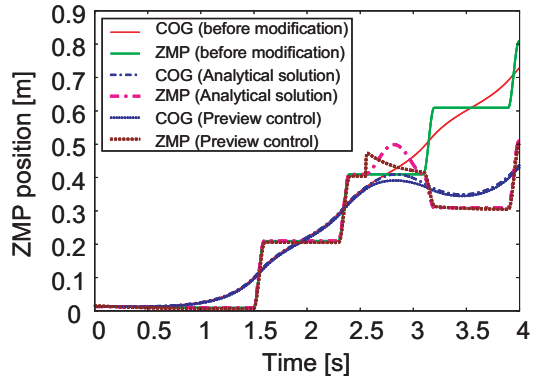

Fig. 2. Immediate modification of foot placement. Solid lines correspond to a first set of input steps. The dashed lines correspond to a second set, where the third step (from t=3s to t=3.8s) has been changed. For the dotted lines, the same modification of the third step is required at time t=2.5s.

control loop. However, the response of this dedicated solver is inadequate in case of modification of the trajectories that happens just before the change of foot support, and for quick changes of the disturbance. Yet, these problems corresponds to the good behavior of the feedback controller.

In this paper, we therefore propose to combine the two approaches in an unified framework. First the ideal states of the COG and the ZMP are calculated from past foot placement. The disturbance is defined as the difference between the ideal and the current states. This disturbance is typically due to external forces. The small disturbance or that appears during the late period of the single-support phase, is mainly suppressed by the state feedback. The large disturbance and at first period of the single-support phase, is absorbed by modifying reactively the next steps, using the dedicated analytical solver.

II. Ideal COG and ZMP trajectories

To generate the COG and the ZMP trajectories online, the linear-inverted-pendulum model (LIPM) is widely used. The dynamics of LIPM is expressed as a set of second-order differential equations. This characteristic system is known as *non-minimum phase*. It has a performance limitation because of unavoidable undershoot in time domain [13].

The problem can then be solved by working on the trajectories of both COG and ZMP, by solving a boundary-value problem [10]. However, the classical solution to solve this problem cannot decide in the same time the foot placements. Indeed, foot placements are generally considered as an input of the solver, not as an output. This solution is referred as *preview control* in the following.

To decide simultaneously the trajectories and the optimal foot placements, the analytical solver [9] presented upper can be used. When more than two future steps are given without immediate modification of foot placement, there is very few fluctuation of the ZMP (i.e. the obtained ZMP trajectory is very close to the reference one – Fig. 2, solid line). However, if a modification in the very near future, it can cause strong fluctuation of the COG and the ZMP trajectories, as shown in Fig. 2 with the analytical solution (dotted line) and with the preview control (dashed lines).

The COG and the ZMP trajectories without the ZMP fluctuation are defined as ideal trajectories. The ideal trajectories do not necessarily correspond to the current state (i.e. current position and the velocity of the COG and the ZMP). The difference between the current and ideal states are regarded as errors that should be suppressed by a state-feedback controller.

III. Disturbance suppression by state feedback

In the following discussion, we only discuss the biped walking pattern in sagittal plane, as shown in Fig. 3. The biped walking pattern in frontal plane, however, can be derived in a similar way.

A. Open-loop dynamical equation

As shown in Fig. 3-(a), the pelvis is assumed to move horizontally. Its dominant dynamics can then be approximated to the dynamics of carted inverted pendulum [11], which is linear:

$$\ddot{x} = \omega^2(x - p_x), \tag{1}$$

$$\omega := \sqrt{\frac{g}{z}}, \tag{2}$$

where x is the (current) horizontal position of the COG, p_x denotes the (current) ZMP position and ω is natural angular frequency of the inverted pendulum. g is the gravity acceleration. The ideal COG and ZMP trajectories (given by the preview control) are also generated from the LIPM dynamical system. Therefore their dynamics can be represented by a similar equation:

$$\ddot{x}^{ideal} = \omega^2(x^{ideal} - p_x^{ideal}). \tag{3}$$

Finally, the disturbance is also approximate to the same dynamics:

$$\ddot{x}^{dis} = \omega^2(x^{dis} - p_x^{dis}), \tag{4}$$

where

$$x^{dis} = x - x^{ideal},$$
$$p_x^{dis} = p_x - p_x^{ideal}.$$

The ZMP is equivalent to a virtual cart which moves within the support polygon, as shown in Fig.3 (b). From this comparison, we suppose in the following that the ZMP speed can be directly controlled by the input u_x.

$$\dot{p}_x^{dis} = u_x \tag{5}$$

The state of the system is then the COG position and velocity, and the ZMP position. From (4) and (5), the state-space system is directly obtained:

$$\frac{d}{dt}\begin{bmatrix} x^{dis} \\ \dot{x}^{dis} \\ p_x^{dis} \end{bmatrix} = \begin{bmatrix} 0 & 1 & 0 \\ \omega^2 & 0 & -\omega^2 \\ 0 & 0 & 0 \end{bmatrix}\begin{bmatrix} x^{dis} \\ \dot{x}^{dis} \\ p_x^{dis} \end{bmatrix} + \begin{bmatrix} 0 \\ 0 \\ 1 \end{bmatrix} u_x \ , \tag{6}$$

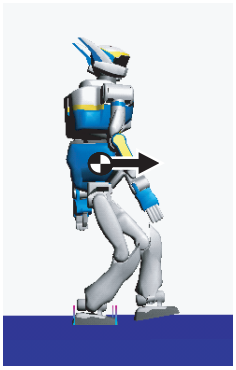

(a) Biped humanoid walking

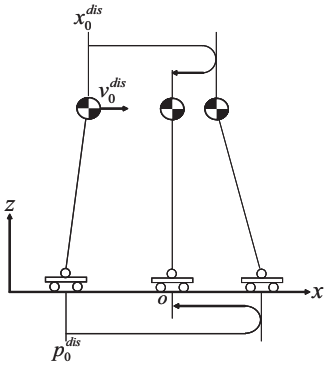

(b) Carted inverted pendulum model

Fig. 3. Model of biped humanoid walking

B. Close-loop equation

The following state-feedback control law is applied to the system (6):

$$u_x = -k_1 x^{dis} - k_2 \dot{x}^{dis} - k_3 p_x^{dis}, \tag{7}$$

where k_1,k_2,and k_3 are arbitrary feedback gains. To be stabilized, adequate feedback gains have to be selected, as done in the following section.

From (6) and (7), the characteristic equation of the closed loop system is derived as

$$\psi(s) \quad = \quad s^3 - k_3 s^2 + \omega^2(k_2 - 1)s + \omega^2(k_1 + k_3). \tag{8}$$

where s denotes the Laplace-transform variable

C. Feedback-gain identification

The three real poles of the closed-loop system are denoted by α, β and γ ($\alpha, \beta, \gamma < 0$). If the three poles exist, the characteristic equation is:

$$\begin{aligned} \psi(s) &= (s-\alpha)(s-\beta)(s-\gamma) \\ &= s^3 - (\alpha+\beta+\gamma)s^2 + (\alpha\beta + \alpha\gamma + \beta\gamma)s - \alpha\beta\gamma. \end{aligned} \tag{9}$$

By identification of the coefficients of (10) from (8), the feedback gains ensuring the three given real poles can be rewritten:

$$\begin{aligned} k_1 &= -\alpha - \beta - \gamma - \frac{\alpha\beta\gamma}{\omega^2} \\ k_2 &= \frac{\alpha\beta + \beta\gamma + \alpha\gamma}{\omega^2} + 1 \\ k_3 &= \alpha + \beta + \gamma \end{aligned}$$

The gains can now be decided by selecting the appropriate poles.

D. Pole selection

In [15], a similar controller tuning was presented, based on the pole assignment of the LIPM close-loop response. The controller was set to maximize standing stable region.

Rather than maximizing the stable region, the selection of the appropriate poles can be decided as a minimization

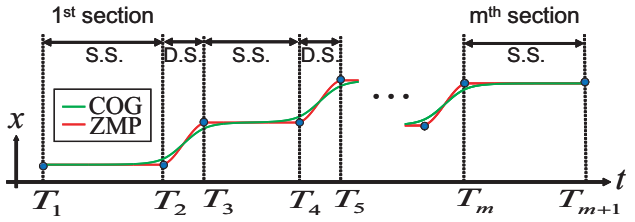

Fig. 4. The COG and The ZMP trajectories

the maximum ZMP peak. This minimization is obtained if selecting one pole near the natural frequency of the inverted pendulum and the two others set on the left half plane, either as close or as far to the origin as possible [14]. When sent to the limit, the three poles are set to

$$\{\alpha, \beta, \gamma\} \to \{0, -\omega, -\infty\},$$

At the limit, the ZMP response becomes a constant value respecting the initial state conditions (initial position x_0 and velocity v_0 of the COG). This constant ZMP position corresponds trivially to the minimum peak.

$$p_x(t) \quad = \quad x_0 + \frac{v_0}{\omega} \tag{10}$$

IV. Reactive step based on an analytical solution

A. COG analytical trajectory

At first, the bipedal gait is divided into several segments for each single support (S.S.) and double support phases (D.S.), as shown in Fig. 4. For each segment, the ZMP reference trajectory is modelized by a third-order ZMP polynomial. The COG trajectory corresponding to the ZMP reference and respecting the dynamics of the LIPM is then analytically deduced.

At j-th segment, the ZMP $p_x^{(j)}$ is assumed to be represented by cubic polynomial:

$$p_x^{(j)}(t) \quad = \quad a_0^{(j)} + a_1^{(j)}\Delta t_j + a_2^{(j)}\Delta t_j^2 + a_3^{(j)}\Delta t_j^3 \tag{11}$$

where $\Delta t_j = t - T_j$ is the relative time to the segment initial time T_j and the $a_i^{(j)}$ are the coefficients of the polynomial. The $a_i^{(j)}$ are determined from the boundary and connectivity conditions of the trajectory of the COG and the ZMP.

As previously, the COG height is assumed to be constant on each segment. Its value is then calculated by the average of initial and terminal value of the segment.

$$\tilde{z}_j = \frac{1}{2}\{(z(T_{j+1}) - p_z(T_{j+1})) - (z(T_j) - p_z(T_j))\}$$

Equation (2) then becomes:

$$\omega_j = \sqrt{\frac{g}{\tilde{z}_j}}. \tag{12}$$

From (1), (11) and (12), the COG trajectory $x^{(j)}(t)$ on the segment can be analytically derivated:

$$\begin{aligned} x^{(j)}(t) &= V^{(j)}\cosh(\omega_j \Delta t_j) + W^{(j)}\sinh(\omega_j \Delta t_j) \\ &+ \left(a_0^{(j)} + \frac{2}{\omega_j^2}a_2^{(j)}\right) + \left(a_1^{(j)} + \frac{6}{\omega_j^2}a_3^{(j)}\right)\Delta t_j \\ &+ a_2^{(j)}(\Delta t_j)^2 + a_3^{(j)}(\Delta t_j)^3 \end{aligned} \tag{13}$$

Substituting the initial position and velocity of the COG $x^{(j)}(T_j)$, $\dot{x}^{(j)}(T_j)$, the initial ZMP $p_x^{(j)}(T_j)$, $\dot{p}_x^{(j)}(T_j)$ and the terminal ZMP $p_x^{(j)}(T_{j+1})$, $\dot{p}_x^{(j)}(T_{j+1})$ at j-th segment into (11), (13) and its derivatives, all of coefficients can be analytically obtained:

$$\begin{aligned}
V^{(j)} &= x^{(j)}(T_j) - p_x^{(j)}(T_j) - \frac{2}{\omega_j^2} a_2^{(j)} \\
W^{(j)} &= \frac{1}{\omega_j}\left(\dot{x}^{(j)}(T_j) - \dot{p}_x^{(j)}(T_j) - \frac{6}{\omega_j^2} a_3^{(j)}\right) \\
a_0^{(j)} &= p_x^{(j)}(T_j) \\
a_1^{(j)} &= \dot{p}_x^{(j)}(T_j) \\
a_2^{(j)} &= \frac{1}{(\Delta T_j)^2}\Big\{3(p_x^{(j)}(T_{j+1}) - p_x^{(j)}(T_j)) \\
&\quad -(\dot{p}_x^{(j)}(T_{j+1}) + 2\dot{p}_x^{(j)}(T_j))\Delta T_j\Big\} \\
a_3^{(j)} &= \frac{1}{(\Delta T_j)^3}\Big\{-2(p_x^{(j)}(T_{j+1}) - p_x^{(j)}(T_j)) \\
&\quad +(\dot{p}_x^{(j)}(T_{j+1}) + \dot{p}_x^{(j)}(T_j))\Delta T_j\Big\}.
\end{aligned}$$

where $\Delta T_j = T_{j+1} - T_j$.

B. Boundary conditions

In the following, we denote $\boldsymbol{X}(T_{j+1})$ the COG state: $\boldsymbol{X}(T_j) = \left[x^{(j)}(T_j)\ \dot{x}^{(j)}(T_j)\right]^T$. Similarly, the ZMP position and velocity is denoted: $\boldsymbol{p}(T_j) = \left[p_x^{(j)}(T_j)\ \dot{p}_x^{(j)}(T_j)\right]^T$. From the analytical coefficients that define the ZMP and COG trajectories, the terminal COG state $\boldsymbol{X}(T_{j+1})$ can be expressed in function of the initial COG state $\boldsymbol{X}(T_j)$ and the boundary conditions of the ZMP $\boldsymbol{p}(T_j), \boldsymbol{p}(T_{j+1})$:

$$\boldsymbol{X}(T_{j+1}) = \boldsymbol{A}^{(j)}\boldsymbol{X}(T_j) + \begin{bmatrix} \boldsymbol{B}_1^{(j)} & \boldsymbol{B}_2^{(j)} \end{bmatrix} \begin{bmatrix} \boldsymbol{p}(T_j) \\ \boldsymbol{p}(T_{j+1}) \end{bmatrix}$$

where the $\boldsymbol{A}$ and $\boldsymbol{B}$ matrices are defined as follow:

$$\begin{aligned}
\boldsymbol{A}^{(j)} &= \begin{bmatrix} c_j & \frac{s_j}{\omega_j} \\ \omega_j s_j & c_j \end{bmatrix} \\
\boldsymbol{B}_1^{(j)} &= \begin{bmatrix} \frac{(6-\omega_T^2)c_j+6}{\omega_T^2} - \frac{12 s_j}{\omega_T^3} & \frac{2(2c_j+1)}{\omega_j \omega_T} - \frac{(6+\omega_T^2)s_j}{\omega_j \omega_T^2} \\ \frac{\omega_j(6-\omega_T^2)s_j}{\omega_T^2} - \frac{12\omega_j c_j}{\omega_T^3} & \frac{4 s_j}{\omega_T} - \frac{(6+\omega_T^2)c_j}{\omega_T^2} \end{bmatrix}, \\
\boldsymbol{B}_2^{(j)} &= \begin{bmatrix} \frac{-6c_j-6+\omega_T^2}{\omega_T^2} + \frac{12 s_j}{\omega_T^3} & \frac{2c_j+4}{\omega_j \omega_T} - \frac{6}{\omega_j \omega_T^2} \\ -\frac{6\omega_j s_j}{\omega_T^2} + \frac{12\omega_j c_j}{\omega_T^3} & \frac{2 s_j}{\omega_T} - \frac{6 c_j}{\omega_T^2} \end{bmatrix},
\end{aligned}$$

with $\omega_T \equiv \omega_j \Delta T_j$.

C. Boundary-condition propagation

The boundary conditions can be then propagated, since the ending condition of segment j is the initial condition of segment $j+1$. Substituting the terminal COG at j-th segment into the initial COG at $j+1$-th segment sequentially, the terminal COG at last m-th segment can be obtained:

$$\boldsymbol{X}(T_{m+1}) = \widehat{\boldsymbol{A}}^{(m)}\boldsymbol{X}(T_1) + \widehat{\boldsymbol{B}}^{(m)}\boldsymbol{P} \tag{14}$$

where

$$\begin{aligned}
\boldsymbol{P} &= \begin{bmatrix} \boldsymbol{p}^T(T_1) & \cdots & \boldsymbol{p}^T(T_m) & \boldsymbol{p}^T(T_{m+1}) \end{bmatrix}^T \\
\widehat{\boldsymbol{A}}^{(m)} &= \prod_{i=m}^{1} \boldsymbol{A}^{(i)} \\
\widehat{\boldsymbol{B}}^{(m)} &= \Bigg[\left(\prod_{i=m}^{2} \boldsymbol{A}^{(i)}\right)\boldsymbol{B}_1^{(1)} \\
&\quad \left(\prod_{i=m}^{3} \boldsymbol{A}^{(i)}\right)\left(\boldsymbol{A}^{(2)}\boldsymbol{B}_2^{(1)} + \boldsymbol{B}_1^{(2)}\right) \\
&\quad \cdots \quad \boldsymbol{A}^{(m)}\boldsymbol{B}_2^{(m-1)} + \boldsymbol{B}_1^{(m)} \quad \boldsymbol{B}_2^{(m)} \Bigg]
\end{aligned}$$

D. ZMP boundary conditions from foot placement

Three steps at least are assumed to be preplanned (if less, the missing foot placement can be set to 0). The number of segment m becomes $2n+1$ for n-th steps when currently in single support and $2n+2$ in double support. Only the single support phase is discussed, since the same same approach is valid in double support.

The desired ZMP trajectory $\boldsymbol{x}_{zmp} = [p_x\ p_y\ p_z]^T$ during segment k can be determined from the corresponding desired foot placement $\boldsymbol{x}_f^{(k)} = [x_f^{(k)}\ y_f^{(k)}\ z_f^{(k)}]^T$.

$$\boldsymbol{x}_{zmp}(T_{2k-1}) = \boldsymbol{x}_f^{(k)} + \boldsymbol{R}_f^{(k)}\boldsymbol{x}_{ini} \tag{15}$$

$$\boldsymbol{x}_{zmp}(T_{2k}) = \boldsymbol{x}_f^{(k)} + \boldsymbol{R}_f^{(k)}\boldsymbol{x}_{end} \tag{16}$$

for $k = 2 \ldots [(m+1)/2]$, where $\boldsymbol{R}_f^{(k)} \in \Re^{3\times 3}$ is the desired attitude of the sole, $\boldsymbol{x}_{ini} = [x_{ini}\ y_{ini}\ z_{ini}]$ and $\boldsymbol{x}_{end} = [x_{end}\ y_{end}\ z_{end}]^T$ denote the initial and terminal ZMP offsets from the sole origin.

The desired ZMP velocity at each segment bounds is set to 0:

$$\dot{p}_x(T_{2k-1}) = \dot{p}_x(T_{2k}) = \dot{p}_y(T_{2k-1}) = \dot{p}_y(T_{2k}) = 0. \tag{17}$$

From (15) - (17), the condition due to foot placements can be rewritten as:

$$\boldsymbol{P}_{3\to m+1} = \boldsymbol{K}\boldsymbol{x}_f + \boldsymbol{P}_{offset}, \tag{18}$$

where

$$\begin{aligned}
\boldsymbol{P}_{3\to m+1} &= \Big[\ p_x(T_3)\ \ 0\ \ p_x(T_4)\ \ 0\ \ \cdots \\
&\qquad \cdots\ \ p_x(T_m)\ \ 0\ \ p_x(T_{m+1})\ \ 0\ \Big]^T, \\
\boldsymbol{x}_f &= \begin{bmatrix} x_f^{(3)} & \cdots & x_f^{([(m+1)/2])} \end{bmatrix}^T, \\
\boldsymbol{P}_{offset} &= \Big[\ \bar{x}_{ini}^{(3)}\ \ 0\ \ \bar{x}_{end}^{(3)}\ \ 0\ \ \cdots \\
&\qquad \cdots\ \ \bar{x}_{ini}^{([(m+1)/2])}\ \ 0\ \ \bar{x}_{end}^{([(m+1)/2])}\ \ 0\ \Big]^T, \\
\boldsymbol{K} &= \begin{bmatrix} 1 & 0 & 1 & 0 & 0 & 0 & \cdots & & 0 \\ 0 & 0 & 0 & 1 & 0 & 1 & 0 & & \vdots \\ \vdots & & & 0 & & \ddots & & \ddots & 0 \\ 0 & & & \cdots & & 0 & 0 & 1\ \ 0 & 1 \end{bmatrix}^T.
\end{aligned}$$

E. Analytic LIPM constraint from foot placement

Substituting (17) and (18) into (14), the relation between the initial COG and ZMP, their evolution along the next steps and the placement of the feet can finally be obtained:

$$\begin{aligned} \boldsymbol{X}(T_{m+1}) &= \widehat{\boldsymbol{A}}^{(m)}\boldsymbol{X}(T_1) + \widehat{\boldsymbol{B}}^{(m)}_{ini}\boldsymbol{P}_{ini} \\ &\quad + \widehat{\boldsymbol{B}}^{(m)}_{3\to m+1}(\boldsymbol{K}\boldsymbol{x}_f + \boldsymbol{P}_{offset}) \end{aligned} \quad (19)$$

where the terminal position of the COG is set equals to the last foot placement, a 0 terminal velocity of the COG:

$$\begin{aligned} x(T_{m+1}) &= x_f^{([(m+1)/2])} \\ \dot{x}(T_{m+1}) &= 0 \end{aligned}$$

This condition gives the constraint that link the evolution of the COG of the LIPM to the placement of the next feet, when the ZMP is selected as (15)-(16).

F. Automatic foot placement

Then the foot placements can be calculated automatically as a solution of a quadratic programming problem under the previous constraint:

$$\min_{\boldsymbol{x}_f} \frac{1}{2}(\boldsymbol{x}_f - \boldsymbol{x}_f^{ref})^T\boldsymbol{Q}(\boldsymbol{x}_f - \boldsymbol{x}_f^{ref}) \quad (20)$$

$$\text{subject to } (19)$$

where, $\boldsymbol{x}_f^{ref}$ are the desired foot placements, $\boldsymbol{Q}$ is a (positive definite symmetric) weight matrix, that set the relative importance of the feet. The solution of this minimization problem can be analytically calculated as

$$\boldsymbol{x}_f = \boldsymbol{x}_f^{ref} - \boldsymbol{Q}\boldsymbol{M}^T(\boldsymbol{M}\boldsymbol{Q}^{-1}\boldsymbol{M}^T)^{-1}(\boldsymbol{M}\boldsymbol{x}_f^{ref} - \boldsymbol{N}) \quad (21)$$

where

$$\begin{aligned} \boldsymbol{M} &= \widehat{\boldsymbol{B}}^{(m)}_{3\to m+1}\boldsymbol{K} \\ \boldsymbol{N} &= \boldsymbol{X}(T_{m+1}) - \widehat{\boldsymbol{A}}^{(m)}\boldsymbol{X}(T_1) - \widehat{\boldsymbol{B}}^{(m)}_{ini}\boldsymbol{P}_{ini} \\ &\quad - \widehat{\boldsymbol{B}}^{(m)}_{3\to m+1}\boldsymbol{P}_{offset} \end{aligned}$$

There is no guarantee that the solution of (21) satisfies any additional constraints such as self collision or joint limitations. These constraints can be considered in a second time by a feasible pattern generation method, also available on line [21].

V. Combining Disturbance Suppression and Reactive Step

A. External force estimation

In the previous section, the robot was supposed to move only because of its own motor torques and the reaction of the ground. We now consider the case where the robot is pushed by an extra external forces, seen as a disturbance to be compensated to ensure balance. In a first time, it is necessary to identify this disturbance.

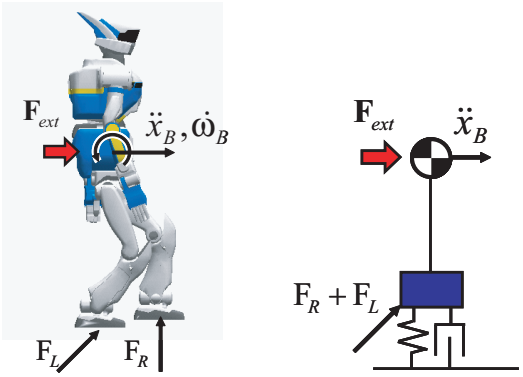

(a) Strict model (b) Simplified model

Fig. 5. Model of external force estimation

The dynamics of the base link of a floating system (such as the humanoid robot) (Fig. 5 (a)) can be written as follows:

$$\begin{aligned} &\begin{bmatrix} \boldsymbol{H}_{11} & \boldsymbol{H}_{12} \\ \boldsymbol{H}_{21} & \boldsymbol{H}_{22} \end{bmatrix}\begin{bmatrix} \ddot{\boldsymbol{x}}_B \\ \dot{\boldsymbol{\omega}}_B \end{bmatrix} + \begin{bmatrix} \boldsymbol{H}_{13} \\ \boldsymbol{H}_{23} \end{bmatrix}\ddot{\boldsymbol{q}} + \begin{bmatrix} \boldsymbol{B}_1 \\ \boldsymbol{B}_2 \end{bmatrix} \\ &= \begin{bmatrix} \boldsymbol{F}_{ext} \\ \boldsymbol{N}_{ext} \end{bmatrix} + \sum_{i=R,L}\begin{bmatrix} \boldsymbol{J}_{1i}^T \\ \boldsymbol{J}_{2i}^T \end{bmatrix}\begin{bmatrix} \boldsymbol{F}_i \\ \boldsymbol{N}_i \end{bmatrix}, \end{aligned} \quad (22)$$

where $\ddot{\boldsymbol{x}}_B$ and $\dot{\boldsymbol{\omega}}_B$ are the linear and angular acceleration of the base link, $\boldsymbol{q}$ are the joint angles, the $\boldsymbol{H}_{ij}$ denote the inertia matrices, $\boldsymbol{B}_i$ are the nonlinear terms (gravity and Coriolis). $\boldsymbol{J}_{1i}$ and $\boldsymbol{J}_{2i}(i = R, L)$ are the Jacobian which relates the velocities of the base link and the left and right feet. $\boldsymbol{F}_{ext}$ and $\boldsymbol{N}_{ext}$ are the external force and torque expressed directly at the base point, and $\boldsymbol{F}_i$ and $\boldsymbol{N}_i$ are the reaction forces and torques of the ground on the left and right feet.

In the case of our humanoid robot, the external forces can not be measured directly, since there is no appropriate force sensors available. However, from the upper row of (22), the external force can be obtained as a function of the other values:

$$\begin{aligned} \boldsymbol{F}_{ext} &= \boldsymbol{H}_{11}\ddot{\boldsymbol{x}}_B + \boldsymbol{H}_{12}\dot{\boldsymbol{\omega}}_B + \boldsymbol{H}_{13}\ddot{\boldsymbol{q}} \\ &\quad + \boldsymbol{B}_1 - \boldsymbol{J}_{1R}^T[\boldsymbol{F}_R^T\ \boldsymbol{N}_R^T]^T - \boldsymbol{J}_{1L}^T[\boldsymbol{F}_L^T\ \boldsymbol{N}_L^T]^T, \end{aligned} \quad (23)$$

All the right-side terms are available by measurements. The acceleration of the base link $\ddot{\boldsymbol{x}}_B, \dot{\boldsymbol{\omega}}_B$ can be estimated from the inertial sensors. The joint acceleration $\ddot{\boldsymbol{q}}$ can be estimated from the joint encoders. And the reaction forces of ground $\boldsymbol{F}_R$ and $\boldsymbol{F}_L$ are directly measured by the force sensors in each ankle.

The external forces acting on the humanoid robot are supposed to be single-point contact. Moreover, the dominant motion is generally due to the own body acceleration and the gravity effect. The Jacobian concerned with the external force becomes only $\boldsymbol{J}_{1i}^T = [\boldsymbol{I}_{3\times 3}\ \boldsymbol{0}]$. Thus, the exact model of Fig. 5-(a) can be simplified as shown in Fig. 5-(b). The external force can then be approximated by:

$$\boldsymbol{F}_{ext} \approx M(\ddot{\boldsymbol{x}}_B + \boldsymbol{g}) - \boldsymbol{F}_R - \boldsymbol{F}_L, \quad (24)$$

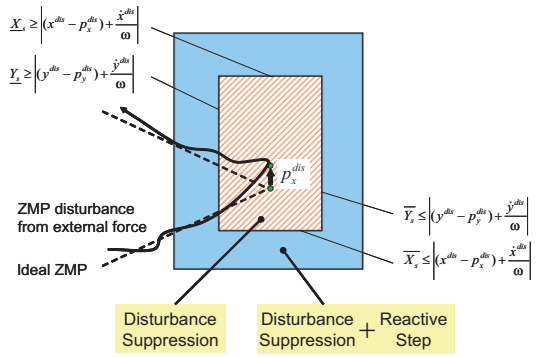

Fig. 6. Motion area

where M is the total mass of the robot and $\boldsymbol{g}$ is the gravity acceleration. Because the external-forces equation includes some measurement noise, the external force is finally estimated through a low-pass filter:

$$\widehat{\boldsymbol{F}}_{ext} = \frac{g_{LPF}}{s + g_{LPF}} \boldsymbol{F}_{ext} \tag{25}$$

where g_{LPF} denotes the arbitrary cut-off frequency.

The external force is computed at the basis of the robot. For being accounted by both the disturbance suppression and the COG trajectory generation, it has to be expressed by its effect on the ZMP. The external force can be converted to a ZMP disturbance by:

$$p_x^{dis} = -\frac{((\boldsymbol{x}_B^{ref} - \boldsymbol{x}_{zmp}^{ref}) \times \widehat{\boldsymbol{F}}_{ext})_y}{\hat{F}_{z,ext}} \tag{26}$$

$$p_y^{dis} = \frac{((\boldsymbol{x}_B^{ref} - \boldsymbol{x}_{zmp}^{ref}) \times \widehat{\boldsymbol{F}}_{ext})_x}{\hat{F}_{z,ext}} \tag{27}$$

B. Disturbance bandwidth distribution

A large external force can not be easily suppressed by any state feedback, especially if applied statically during a long time, due to the limitations of the horizontal motion of a trunk. On the other hand, it is difficult for the swing leg to execute a large motion just before landing. Furthermore if an extra step is used to compensate a small external force without using any feedback suppression, the robot moves during all the step and consumes a lot of energy. Therefore, it is logical to distribute the action of each way to adequately compensate the disturbance, according to its frequency or the situation of the support phase.

As a result of the theoretical minimization of the maximum ZMP peak in (10), the disturbance can be suppressed by only feedback control if the disturbance is satisfied the following ranges:

$$\begin{aligned} \underline{X}_s \leq\ & (x^{dis}(t) - p_x^{dis}(t)) + \frac{\dot{x}^{dis}(t)}{\omega} \leq \overline{X}_s, \\ \underline{Y}_s \leq\ & (y^{dis}(t) - p_y^{dis}(t)) + \frac{\dot{y}^{dis}(t)}{\omega} \leq \overline{Y}_s, \end{aligned}$$

where, $\underline{X}_s$, $\overline{X}_s$, $\underline{Y}_s$ and $\overline{Y}_s$ denote respectively the lower, upper, left and right limitations of the support polygon. This equation can then be used as a selector. The distribution between what goes to the state feedback and to the reactive step is performed through a selection variable α. In case of out of upper limitation $\overline{X}_s$, the distribution ratio α becomes:

$$\alpha = \frac{(x^{dis} - p_x^{dis}) + \frac{\dot{x}^{dis}}{\omega} - \overline{X}_s}{(x^{dis} - p_x^{dis}) + \frac{\dot{x}^{dis}}{\omega}} \tag{28}$$

The ratio is similarly obtained in case of overshoot on the lower, left and right bounds.

The suppression of the disturbance allocated to the state-feedback controller is strait forward.

For the reactive step, the disturbances of the COG position and velocity are added to the initial position and velocity of the COG for the reactive step in (21).

$$\begin{aligned} x(T_1) &\leftarrow x(T_1) + \alpha x^{dis}, \\ \dot{x}(T_1) &\leftarrow \dot{x}(T_1) + \alpha \dot{x}^{dis}, \end{aligned}$$

VI. Experimental results

To confirm the effectiveness of the proposed method, experimention was done by humanoid robot HRP-2 [22]. Original walking pattern was generated with 0.8[s] step cycle. External force was acted by human pushing. Snapshots of experimention are shown in Figure. 7. Each shanpshot was transited every 0.5[s]. Experimental result shows that HRP-2 could respond to the external force in any direction. However HRP-2 could not recover against any strength of the external force or its timing. Especially it was still difficult to maintain a balance during the late period of the single-support phase when a large external force is acted on the robot.

VII. Conclusion and future works

In this paper, we presented a complete solution to couple in a unified framework both the state feedback controller and the reactive stepping. The disturbance, estimated through a simplified model of the robot, is first saturated on the ideal frequency response of the state controller. The overshooting part is then allocated to the reactive stepping, to decide the next foot placements. Finally, the ideal COG and ZMP trajectories are continuously tracked to ensure a proper behavior. The validity of the method was demonstrated through by real experiments on the humanoid robot. The robot was demonstrated to be able compensate for a strong unexpected push during the walk.

The obtained results are very satisfying. However, it should be possible to improve the accuracy of the external-force estimation, for example by relying on a more complete model of the robot. We also suggest to decouple more properly the proposed method and the control of the stabilization. Finally, it may be necessary to account for the attitude error (mainly inclination of the robot chest) at the landing of the swing leg, to reduce the impact when the perturbation strongly acts on the ankle flexibilities.

VIII. Acknowledgments

This research has been partially supported by the JST Strategic Japanese-French Cooperative Program under the name "Robot motion planning and execution through on-line information structuring in real-world environment".

Fig. 7. Snapshot of reactive step by proposed method

REFERENCES

[1] Shuuji Kajita, Fumio Kanehiro, Kenji Kaneko, Kazuhito Yokoi, and Hirohisa Hirukawa, "The 3D linear inverted pendulum mode: a simple modeling for a biped walking pattern generation," *in Proc. of IEEE Int. Conf. on Intelligent Robots and Systems (IROS)*, pp.239-246, 2001.

[2] H. Miura, and I. Shimoyama, "Dynamic walk of a biped," *Int. Jour. of Robotics Research*, Vol.3, No.2, pp.60-74, 1984

[3] T. Komura, H. Leung, S. Kudoh, and J. Kuffner, "A Feedback Controller for Biped Humanoids that Can Counteract Large Purterbations During Gait," *in Proc. of IEEE Int. Conf. on Robotics and Automation*, pp.1989-1995, 2005.

[4] K. Nishiwaki, and S. Kagami, "High Frequency Walking Pattern Generation based on Preview Control of ZMP," *in Proc. of IEEE Int. Conf. on Robotics and Automation*, pp.2667-2672, 2006.

[5] J. Pratt, J. Carff, S. Drakunov, and A. Goswami, "Capture Point: A Step toward Humanoid Push Recovery," *in Proc. of IEEE-RAS Int. Conf. on Humanoid Robots*, pp.200-207, 2006.

[6] H. Diedam, D. Dimitrov, P. B. Wieber, K. Mombaur, and M. Diehl, "Online Walking Gait Generation with Adaptive Foot Positioning through Linear Model Predictive Control," *in Proc. of IEEE/RSJ Int. Conf. on Intelligent Robotics and Systems*, pp.1121-1126, 2008.

[7] R. Tajima, D. Honada, and K.Suga, "Fast Running Experiments Involving a Humanoid Robot," *in Proc. of IEEE Int. Conf. on Robotics and Automation*, pp.1571-1576, 2009

[8] T. Takenaka, T. Matsumoto, T. Yoshiike, T. Hasegawa, S. Shirokura, H. Kaneko and A. Orita, "Real Time Motion Generation and Control for Biped Robot -4th Report: Integrated Balance Control-," *in Proc. of IEEE Int. Conf. on Intelligent Robots and Systems (IROS)*, pp.1601-1608, 2009

[9] M. Morisawa, K. Harada, S. Kajita, K. Kaneko, J. Sola, E. Yoshida, N. Mansard, K. Yokoi, J-P. Laumond, "Reactive stepping to prevent falling for humanoid robots," *in Proc. of IEEE Int. Conf. on Humanoids*, pp.528-534, 2009.

[10] S. Kajita, et al., "Biped Walking Pattern Generation by using Preview Control of Zero-Moment Point," in Proc. of IEEE Int. Conf. on Robotics and Automation, pp.1620-1626, 2003.

[11] T. Sugihara, Y. Nakamura, and H. Inoue, "Realtime Humanoid Motion Generation through ZMP Manipulation based on Inverted Pendulum Control," in Proc. of IEEE Int. Conf. on Robotics and Automation, pp.1404-1409, 2002.

[12] T. Sugihara, "Simulated Regulator to Synthesize ZMP Manipulation and Foot Location for Autonomous Control of Biped Robots," *in Proc. of IEEE Int. Conf. on Robotics and Automation*, pp.1264-1269, 2009

[13] N. Napoleon, H. Nakaura, and M. Sampei, "Balance Control Analysis of Humanoid Robot based on ZMP Feedback Control," *in Proc. of IEEE/RSJ Int. Conf. on IROS*, pp.2437-2442, 2002

[14] M. Morisawa, S. Kajita, K. Kaneko, F. Kanehiro, S. Nakaoka, K. Harada, K. Fujiwara, and H. Hirukawa, "Motion Generation of Emergency Stop at Double Support Phase for Humanoid Robot by Pole Assignment (in Japanese)," Journal of the Robotics Society of Japan, vol. 26, no. 4, pp. 341-350, 2008.

[15] T. Sugihara, "Standing Stabilizability and Stepping Maneuver in Planar Bipedalism based on the Best COM-ZMP Regulator," *in Proc. of IEEE Int. Conf. on Robotics and Automation*, pp.1966-1971, 2009

[16] M. Morisawa, K. Harada, S. Kajita, K. Kaneko, F. Kanehiro, K. Fujiwara, S. Nakaoka, and H. Hirukawa, "A Biped Pattern Generation Allowing Immediate Modification of Foot Placement in Real-Time," *in Proc. of IEEE-RAS Int. Conf. Humanoid Robots*, pp.581-586, 2006.

[17] S.A. Setiawan, J. Yamaguchi, J. S.H. Hyon, A. Takanishi, "Physical interaction between human and a bipedal humanoid robot-realization of human-follow walking," *in Proc. of IEEE Int. Conf. on Robotics and Automation*, pp.361-367, 1999.

[18] S.H.Hyon and G.Cheng, S. H. Hyon, J. G. Hale, and G. Cheng, "Full-Body Compliant HumanHumanoid Interaction: Balancing in the Presence of Unknown External Forces," *IEEE Trans. on Robotics and Automation*, Vol. 23, Issue 5, pp.884-898, 2007.

[19] S. Hong, Y. Oh, Y. H. Chang, and B. J. You, "An Omni-directional Walking Pattern Generator Method for Humanoid Robots with Quartic Polynomials," *in Proc. of IEEE/RSJ Int. Conf. on Intelligent Robots and Systems*, pp.4207-4213, 2007.

[20] B. Lee, D. Stonier, Y. Kim, J. Yoo, and J. Kim, "Modifiable Walking Pattern of a Humanoid Robot by Using Allowable ZMP Variation," *IEEE Trans. on Robotics*, Vol. 24, No. 4, pp.917-925, 2008

[21] F. Kanehiro, W. Suleiman, K. Miura, M. Morisawa, E. Yoshida, "Feasible pattern generation method for humanoid robots," *in Proc. of IEEE-RAS Int. Conf. Humanoid Robots*, pp.542-548, 2009.

[22] K.Kaneko, et al., "The Humanoid Robot HRP2," *Proc. of IEEE Int. Conf. on Robotics and Automation*, pp.1083-1090, 2004.